

See discussions, stats, and author profiles for this publication at: <https://www.researchgate.net/publication/339055905>

In-plane shear testing of unreinforced masonry walls and comparison with FEA and NZSEE predictions

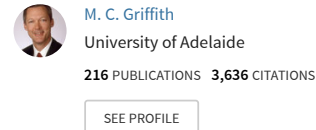
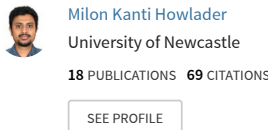
Article in International Journal of Masonry Research and Innovation · January 2020

DOI: 10.1504/IJMRI.2020.104845

CITATIONS
0

READS
53

3 authors, including:



Some of the authors of this publication are also working on these related projects:

-  Cost-Effective Mitigation Strategy Development For Building Related Earthquake Risk [View project](#)
-  children's planning [View project](#)

In-plane Shear Testing of Unreinforced Masonry Walls and Comparison with FEA and NZSEE Predictions

Milon Howlader* and Mark Masia

Centre of Infrastructure Performance and Reliability, The University of Newcastle, Callaghan, NSW 2308, Australia
Email: MilonKanti.Howlader@uon.edu.au
Email: mark.masia@newcastle.edu.au
*Corresponding author

Michael Griffith

School of Civil, Environmental and Mining Engineering, The University of Adelaide, North Terrace Campus, SA 5005, Australia
Email: michael.griffith@adelaide.edu.au

Abstract: Unreinforced masonry (URM) constructions are vulnerable to seismic loading due to their high mass and stiffness and low ductility and tensile strength. It is important to be able to predict the seismic resistance and the governing failure modes of URM walls and components in order to evaluate the seismic hazard for existing URM structures. If local out-of-plane failure mechanisms are restrained via suitable detailing, the capacity against collapse under seismic loading for URM buildings is typically limited to the in-plane shear capacity of the URM walls. Based on observations of damage suffered from previous earthquakes, the present study was conducted to investigate the global and local in-plane response of perforated URM walls under earthquake loading. Full-scale cyclic in-plane testing of URM walls with an arched opening which were designed to represent walls in heritage URM structures in Australia was performed. The study investigated the behaviour of both pier and spandrel elements within the walls. Emphasis was also given to the position of walls within a multi-storey building by varying the pre-compression loads (representing gravity loads) on the walls. The tested walls were then simulated using nonlinear Finite Element analyses (FEA) where simplified micro-modelling (crack-shear-crush) approaches were used to analyse the wall behaviour. Finally, the shear capacities and the failure modes of the walls obtained from the experimental tests and FE analyses were compared to the proposed New Zealand Society for Earthquake Engineering (NZSEE) predictions.

Keywords: Unreinforced masonry (URM), In-plane shear behaviour, cyclic testing, FEA, NZSEE.

Reference to this paper should be made as follows: Howlader, M., Masia, M., Griffith, M. (2018) 'In-plane shear testing of unreinforced masonry walls and comparison with FEA and NZSEE predictions', *Int. J. Masonry Research and Innovation*, Vol. , No , pp.

Biographical notes: Milon Howlader is a Civil Engineer and graduated at Khulna University of Engineering & Technology, Bangladesh in 2009. He has performed several research activities in the structural engineering field after his

graduation. He has published 5 journal and 9 international conference papers as author and co-author in the field of Civil Engineering. In 2015, he completed his Master in sustainable construction under natural hazards and catastrophic events with a thesis on cold-forming effects on stainless steel sections from Czech Technical University in Prague. Since 2016 he is studying for his PhD in Civil Engineering at The University of Newcastle, Australia. His research activities are mainly focused on the seismic assessment of the heritage unreinforced masonry structures in Australia.

Mark Masia is an Associate Professor at The University of Newcastle. He has authored 1 book chapter and more than 100 publications, of them 30 papers are scientific journals. His research interests are to develop improved methods of assessment and design for unreinforced masonry structures and efficient means for retrofitting/strengthening existing masonry structures.

Michael Griffith is a Professor in the School of Civil, Environmental and Mining Engineering at the University of Adelaide. He has authored or co-authored 2 book chapters and over 140 refereed papers in the field of earthquake engineering and structural dynamics. His research has focussed on developing methods to prevent earthquake induced damage, including collapse, of unreinforced masonry buildings and non-seismically designed reinforced concrete frames. He is also currently involved with specialist consultant work for engineering firms in the field of earthquake engineering, is a member of the joint Australia-New Zealand Standards Earthquake Loading committee, and previously worked as a structural engineer in Berkeley, specialising in the earthquake analysis and design of piping systems in nuclear power plants.

*This paper is a revised and expanded version of a paper entitled '**Prediction of in-plane shear capacity of perforated URM walls: nonlinear finite element modelling compared with the NZSEE formula**' presented at **10th International Masonry Conference, 9-11 July, 2018, Milan, Italy.***

1 Introduction

Unreinforced masonry (URM) was the most common form of construction practice in Australia throughout the 19th century and the early 20th century. URM building damage in the Newcastle Central Business District (CBD) due to the 1989 earthquake (M5.6) provided ample evidence of the poor seismic performance of older URM structures in Australia (Melchers and Page, 1990). The vulnerability to earthquakes of URM structures was first taken into consideration for design in Australia after the Meckering earthquake occurred in 1968 (M6.9), resulting in the introduction of the first Earthquake Resistant Buildings standard (AS2121, 1979).

The hazard posed to URM buildings by earthquakes has raised the interest of researchers internationally (Magenes and Calvi, 1997; Moon et al., 2006; Bothara et al., 2010) to develop improved assessment, analysis and appropriate retrofitting techniques for existing structures. However, the diversity of the materials, components, and structural configurations of URM buildings makes it difficult to ascertain the seismic performance for buildings other than the types of structures on which the research was based (Calvi et al., 1996). Generally, older existing URM buildings are composed of several load bearing and partition walls oriented in orthogonal directions with flexible

diaphragms at floor and roof level. The seismic load from the ground is transferred via the footing/foundation to the stiff in-plane loaded URM walls, which are considered as the primary lateral load resisting component, and then transmitted to the out-of-plane walls through flexible floor and roof diaphragms. The out-of-plane walls may also fail during earthquake loading due to excessive deflection of the diaphragm but such localized failures can be minimised by proper tie connection between the walls and diaphragms. Hence, the system of in-plane walls is the most prominent lateral load-bearing system for such structures and their failure governs the total failure of the structure.

The in-plane loaded URM walls often include openings (perforations) to allow for the provision of windows and doors. The openings present in a wall divide the wall into a series of vertical (pier) and horizontal (spandrel) components. Despite much of the past research focusing on the behaviour of URM piers, observations from past earthquakes reveal that damage may also occur in the spandrels. Therefore, the assessment of perforated URM walls subjected to in-plane loading cannot be confined only to consideration of the piers by assuming the spandrel elements possess infinite strength and stiffness. Realising the importance of the behaviour of spandrels on the global behaviour of the perforated URM walls during earthquake loading, full or reduced scale perforated wall testing programs were conducted by various researchers (Yi et al., 2006; Nateghi and Alemi, 2008; Bothara et al., 2010; Augenti et al., 2011; Vanin and Foraboschi, 2012; Triller et al., 2016; Allen et al., 2016; Knox et al., 2017). These testing programs considered both new and old masonry practices in different countries throughout the world. A significant number of numerical analyses on masonry structures have also been carried out by various researchers (Lourenco, 1996 a; Brencich et al., 1998; Lagomarsino et al., 2013; Betti et al., 2014; Allen et al., 2017; Howlader et al., 2018). The numerical analyses most commonly used include finite element micro-modelling or macro-modelling and equivalent frame (EF) approaches in which the nonlinearity and the orthotropy of the masonry was considered.

The current paper reports an experimental testing and numerical modelling study of perforated URM shear walls which focuses on material properties and wall geometries representative of 19th century and early 20th century Australian URM construction. Such construction makes up much of Australia's heritage listed building stock, for which reliable methods for seismic assessment and retrofit are required.

2 Experimental in-plane testing of URM walls

2.1 Specimen geometry

Four URM walls were constructed with the same geometric configuration which comprised two piers connected by a shallow spandrel with a semicircular arched opening as shown in Figure 1. The walls were two leaf thick solid construction with a thickness of 230 mm constructed using the common bond pattern with courses of header bricks used at every fourth course to connect tightly the two leaves of the wall. This geometry was designed to represent a single storey section of wall within a larger perforated masonry façade and to be typical of wall geometries observed in the late 19th and early 20th century construction (Howlader et al., 2016). Two different pre-compression levels of

approximately 0.2 MPa (2.8% f'_m) and 0.5 MPa (7.1% f'_m) were chosen to represent the effect of pier axial stress due to gravity loads on the walls at different positions within a building. The lower pre-compression level represents the wall on the top storey and the higher level for the bottom storey of a three storey building. For each level of pre-compression two wall specimens were tested, resulting in four wall specimens in total. The walls were constructed by professional bricklayers under close supervision. In this paper, the specimens are designated according to wall geometry type_precompression level_test repetition. For example, WS_0.2_1 means shallow spandrel wall with 0.2 MPa precompression stress and 1 is for the first of two tests for this combination.

2.2 Material Properties

The tested specimens were constructed using a low strength dry pressed solid clay brick unit of dimensions 230 mm x 110 mm x 76 mm, chosen to represent, as closely as possible, heritage clay brick masonry in Australia. A weak lime rich cement-lime mortar consisting of 1 cement : 2 lime (rock) : 9 sand by volume was used for all four wall specimens. This mortar falls into the AS3700 'M2' classification (AS3700, 2018), which has low tensile and shear bond strength and can represent the weather deteriorated mortar of the heritage buildings. The mortar bed and head joints and the collar joint between the two masonry leaves were completely filled with mortar with approximate joint thickness equal to 10 mm. The key material properties of the masonry, brick and mortar as measured using the standard test methods are presented in Table 1 below.

The mortar curing time was at least 28 days prior to wall testing and for every batch of mortar used in the wall specimen construction, 10 mortar joints were prepared to determine the masonry flexure bond strength using the bond wrench test in accordance with AS3700 (2018). The direct tensile strength of the mortar joint (f_{jt}) was obtained from the flexural bond strength (f_{sp}) by dividing a factor of 1.5. The values for every batch of mortar used in the wall construction are shown in Table 2.

2.3 Test setup and instrumentation

The test setup for quasistatic cyclic in-plane loading for this experimental program is shown in Figure 2. The vertical pre-compression load was first applied using the vertically aligned hydraulic jack. The vertical load was equally distributed to the centre line of each pier through the spreader beam (250UC 72.9) and was kept constant during the test. Cyclic lateral displacement (Figure 3) was then applied at the mid-length of the loading beam (200UC 46.2). Additional beam sections over the pier length were located below the spreader beam to uniformly distribute the vertical load from the jack to the top of each pier throughout its length. To allow vertical deformation of the spandrel to occur during testing, composite steel sections (300 PFC with top plate and stiffener) were placed between the loading beam and the wall only along the length of each pier, leaving the top edge of the spandrel unrestrained. These composite beam sections were bolted to the loading beam and the bottom surface was attached to the top edge of the wall specimens using high strength epoxy. The steel section sizes and arrangement were designed to create a top of wall boundary condition representative of another masonry

frame above as would occur in a multi-storey URM wall. Further details of the design of the test boundary conditions can be found in Allen et al. (2014).

Lateral force applied to the URM wall was measured using a load cell connected to the lateral hydraulic jack which reacted against a strong wall in the laboratory. The main controlling and monitoring lateral displacement Linear Variable differential transformer (LVDT) was H11 in Figure 2 and other LVDTs were attached at different places of the wall to measure and monitor the displacement during testing (Figure 2). A Digital Image Correlation (DIC) system was also used to record continuous strain and displacement fields over the surface of each wall specimen during testing.

2.4 Summary of the in-plane test observations

The initial observations for all test specimens were nearly the same, wherein cracking initiated in the arch zone and propagated outward into the piers through mortar joints. Cracking formed at the top corner of the left pier for push displacements and top corner of the right pier in the case of pull displacements (push and pull directions are defined in Figure 2). Cracking developed also at the base of the piers to allow pier rocking and with each increase of the lateral displacement, these cracks widened. Significant damage consisting of both flexural and shear cracking through the spandrels was observed in all cases, but at the higher precompression level it was more noticeable. Compressive toe crushing of the piers was observed for both low and high pre-compression levels, except for WS_0.2_1 which did not show any toe crushing of the piers. Where toe crushing was observed, it was most prominent for the higher precompression level.

In case of WS_0.5_2, up until a lateral displacement of ± 24 mm, stable rocking behaviour was observed, similar to the other three specimens. However, during the ± 30 mm cycles in the negative quadrant (pull cycle), diagonal shear failure occurred in the left pier from top to bottom, resulting in sharp strength and stiffness degradation and a wider hysteretic loop at the 36 mm displacement. As the left pier showed shear failure and the right pier showed rocking behaviour, so the hysteretic loop was highly asymmetrical after 30 mm displacement. Also, due to the rocking nature of the right pier, in the positive quadrant (push cycle), there was no significant load drop with increased displacement.

Testing of wall WS_0.5_2 was terminated at 36 mm displacement due to concerns regarding imminent loss of the ability to carry the vertical load. In the other three cases, testing was terminated at drifts of 2% (± 48 mm displacement) prior to any significant post peak strength reduction. For all four specimens, the top brick course slid through the uppermost mortar joint after 24 mm displacement. The vertical movement of the spandrels at ultimate displacement was in between 11-13 mm. The visible cracks at the top and bottom of the piers were first observed at displacements (H11) between 4-6 mm in both push and pull cycles except for WS_0.5_2, where cracking started at 12 mm at the top of the left pier during the push cycle. The crack patterns at the ultimate displacement level for all four tested walls in push direction are shown in Section 5.2.

3 FE Modelling

In the current study, finite element simulation of the URM wall tests was performed using the commercially available software package DIANA 10.2 (Diana FEA, 2017). The simplified micro-modelling strategy was used for modelling the walls whereby the brick units were modelled with continuum elements and the mortar joints, brick/mortar interface and potential brick cracks were modelled using interface elements. As in this approach mortar joints were modelled by zero thickness interface elements, to maintain the actual geometry of the wall, brick units were expanded in both height and length.

Four noded quadratic (Q8MEM) rectangular isoparametric linear plane stress elements with thickness equal to the wall thickness of 230 mm were used for modelling the solid brick units. The interface elements were modelled using four-noded (L8IF) linear interface elements. The brick acted as elastic material surrounded by the potential fracture/slip line through bed & head mortar joints and the potential crack surfaces through brick units. The use of common bond pattern to construct the walls with header units in every fourth course (Figure 1) resulted in a finite element mesh with interface elements representing potential brick crack planes at each quarter length of the bricks. To construct the header courses, the vertical joints were offset from the stretcher courses above and below by one quarter brick length, otherwise the vertical mortar joints would align over three adjacent courses, thus reducing integrity of the wall. Hence, considering the resulting masonry assemblage and to match properly with the nodes of the surrounding elements in the finite element model, potential crack surfaces (interface elements) at each quarter length of the brick were used in this FE modelling. Although the interface elements were of zero thickness in the finite element formulation, for illustrative purposes a fake thickness 5 mm is displayed in the model. The desired vertical precompression load (F_y) was applied through the centre line of each pier in a single step and then held constant. Horizontal displacement (d_x) was then applied at the centre of the loading beam with 480 steps by increasing with constant step size of 0.1 mm up to a maximum of 48 mm deflection. The schematic views of the full wall modelling with the position of the load application are represented in Figure 3.

Most of the material properties used as input parameters in Diana were taken from the material testing at UON laboratory. Some other parameters were taken from the previous author's works, which are referenced in the remarks column in Table 3.

4 URM wall in-plane shear capacity prediction formula

In the current study the strength prediction formulae recommended by NZSEE (2006) and NZSEE (2017) are considered. In both cases, a range of equations are provided, each representing a different potential mode of failure under in-plane lateral loading. Strength prediction requires evaluation of the various formulae, from which the strength, and the governing failure mode, are based on the lowest calculated capacity.

4.1 NZSEE 2006

The basic failure mechanisms due to earthquake loading and the predicted strength according to the failure modes are proposed by the NZSEE (2006) which adopts the expressions by Calvi et al. (1996). In NZSEE (2006), the spandrel is assumed to have infinite strength and stiffness resulting in the failure being confined to the piers. Only the strain limit is proposed for the spandrel where the deflection should not be more than 0.5% of the clear span of the spandrel. The simplified expressions for the strength assessment of the URM pier due to in-plane response considering the importance of various parameters (geometry, material property, axial loading etc) are described below.

The capacity of the wall resisted by the pier rocking (V_r) can be expressed as follows. The shear is carried by the compression masonry and the bed joint cracking occurs in the tension zone.

$$V_r = \frac{N}{h_{eff}} \left(z - \frac{1}{2} \frac{N}{0.85 f_m' b_w} \right) \quad (1)$$

where N is the axial force on the wall cross-section, h_{eff} is the effective height of the pier, z is the distance between the compression edge and the line of action of N (generally the half length of the pier, $l_w / 2$), f_m' is the unconfined masonry compressive strength and b_w is the thickness of the pier.

The strength of the pier due to bed joint sliding (V_s) during earthquake excitation can be calculated as

$$V_s = \frac{3czb_w + \mu_f N}{1 + \frac{3cl_w b_w \alpha_v}{N}} \quad (2)$$

Where l_w is the length of the pier, c is the cohesion, μ_f is the coefficient of friction, and $\alpha_v = \frac{M}{Vl_w}$ which depends on the boundary condition of the pier (Magenes and Calvi, 1997). Other parameters are as stated above.

The maximum shear capacity associated with diagonal cracking considers scenarios where the failure can occur in a stepped pattern through the mortar bed-head joints or directly through the masonry units. The formulation of the shear strength associated with the joint (V_j) and unit (V_b) failures can be expressed as

$$V_j = \frac{cl_w b_w + \mu_f N}{1 + \alpha_v} \quad (3)$$

$$V_b = \frac{\sqrt{f_{bt} l_w b_w (f_{bt} l_w b_w + N)}}{2.3(1 + \alpha_v)} \quad (4)$$

Where f_{bt} is the direct tensile strength of the brick and the other parameters are as stated above.

4.2 NZSEE 2017

The expressions for the horizontal shear strength capacity of solid and perforated URM walls were further refined in NZSEE (2017). The refinement was based on past experimental testing of URM walls (Bothara et al., 2010; Russell, 2010; Knox, 2012; Beyer and Dazio, 2012) and the guidelines of the ASCE 41-13 (2014). The latter code considers the possibility of spandrel failures due to the significant incidence of in-plane spandrel failures observed during earthquakes. For the perforated wall, the seismic capacity assessment is done for both the pier and the spandrel separately and the governing failure mode (lowest resistance) is taken into consideration.

The maximum in-plane rocking capacity (V_r) of the URM wall / pier can be expressed by the following formula. It is one of the stable modes of failure with high deformation capacity.

$$V_r = 0.9(\alpha N + 0.5P_w) \frac{l_w}{h_{eff}} \quad (5)$$

Where α is the factor for boundary condition of the wall/pier (1.0 for fixed-fixed and 0.5 for fixed-free condition), P_w is the self-weight of the wall and the other parameters are as stated above.

Due to the lateral loading, flexural cracking occurs in the tension zone along the bed joint of the wall and the load is carried by the compression toe. The wall starts to rotate about the compression toe trying to overturn the wall and when the compressive stress at the toe exceeds the masonry compressive strength, toe crushing occurs. The maximum toe crushing strength (V_{tc}) can be calculated by the following expression

$$V_{tc} = (\alpha N + 0.5P_w) \left(\frac{l_w}{h_{eff}} \right) \left(1 - \frac{f_a}{0.7f'_m} \right) \quad (6)$$

Where f_a is the axial compressive stress at the base of the wall/pier due to gravity load, f'_m is the masonry compressive strength and the other parameters are as described above.

The bed joint sliding shear strength (V_s) can be calculated as

$$V_s = 0.7 [b_w l_w c + \mu_f (N + P_w)] \quad (7)$$

The shear strength due to diagonal cracking (V_{dt}) can be calculated by the following formula. The cracking occurs when the diagonal tensile strength is exceeded by the principal stress of the wall or pier.

$$V_{dt} = f_{dt} A_n \beta \sqrt{1 + \frac{f_a}{f_{dt}}} \quad (8)$$

Where β is the correction factor for nonlinear stress distribution and depends on the value of (h_{eff}/l_w) , f_a is the axial compressive stress due to gravity load at the mid height

of the wall/pier, f_{dt} is the diagonal tensile strength of the masonry which can be expressed as follows

$$f_{dt} = 0.5c + f_a \mu_f \quad (9)$$

For determining the in-plane strength capacity of the deep arched URM spandrel, it is converted to an equivalent rectangular spandrel by extending the depth to one third of the depth of the arch below the arch apex according to NZSEE (2017). Hence the pier height is taken by extending the straight portion of the pier to two thirds of the arch depth to calculate the shear strength of the pier.

The expected in-plane strength of the URM spandrel due to flexure and shear response is recommended in NZSEE (2017) following Beyer (2012). Beyer (2012) has developed formula to estimate the peak and residual strength of the URM spandrel by considering the typical behavioural mode and the boundary conditions with verification against experimental results of Beyer and Dazio (2012).

The peak shear force ($V_{p,fl}$) due to flexural response and the residual force ($V_{r,fl}$) after the flexure failure of the URM spandrel can be formulated as

$$V_{p,fl} = (f_{t,eq} + p_{sp}) \frac{h_{sp}^2 b_{sp}}{3l_{sp}} \quad (10)$$

$$V_{r,fl} = \frac{p_{sp} h_{sp}^2 b_{sp}}{l_{sp}} \left(1 - \frac{p_{sp}}{0.85 f_{hm}} \right) \quad (11)$$

Where, $f_{t,eq}$ is the equivalent tensile strength of the masonry spandrel, p_{sp} is the mean axial stress in the spandrel, h_{sp} , b_{sp} , l_{sp} are the height, width and clear length of the spandrel respectively.

The peak force ($V_{p,s}$) associated with the shear cracking of the spandrel (where the cracking occurs through the bed and head joints) can be estimated as

$$V_{p,s} = \frac{2}{3} (c + \mu_f p_{sp}) h_{sp} b_{sp} \quad (12)$$

All the parameters are as stated above.

The URM spandrel does not have any residual strength after shear cracking but there is significant residual strength after flexural cracking due to the development of diagonal compression strut through the spandrel.

5 Comparison among experimental results, FEA and NZSEE predictions

5.1 Load displacement behaviour

The lateral force versus displacement relationships of the walls obtained from the experiments are compared to the simulated force displacement relationships obtained from the FEA in Figure 5. The load displacement envelop curves of the tested walls were constructed by connecting the points of the peak loads of the first cycle for each displacement amplitude for both positive and negative directions on the hysteresis loops.

The hysteresis loops for WS_0.2_1 (wall with low precompression load) and for WS_0.5_1 (wall with high precompression load) are shown in Figure 4.

From Figure 5, it is shown that the FEA results are in good agreement with the experimental results showing extensive nonlinearity after the initial linear portion. The FEA results showed higher initial stiffness than the experimental results in all cases but in the case of wall WS_0.2_1, the FEA result was close to the experimentally observed initial stiffness. As the wall WS_0.2_1 was tested after 5 months from the construction date, it is expected that the lime rich mortar is not able to gain its full strength (and stiffness) after 28 days (the other walls were tested at 28 days).

The tests were continued until 48 mm (2% drift) in both positive and negative directions (except for WS_0.5_2 as discussed above) as the loads did not decrease by 20% of the maximum lateral load. In the FEA it is also shown that in the case of low pre compression level, for displacements up to 48 mm, post peak load drop equal to 20% of the maximum load was not attained. However, for the higher pre compression level, at 36.1 mm displacement, the FEA post peak load capacity did fall by more than 20% of the maximum load. This load drop was also shown in the negative (pull) direction of WS_0.5_2 at 35.6 mm displacement.

5.2 Failure modes

The crack patterns observed in the tested walls at the ultimate limit state at push (+) cycles are presented with the FEA predicted failure modes in Figure 6. The crack patterns for the tested walls (Figure 6a, b, d, e) are presented by plotting the contour map of the major principal strain obtained from digital image correlation (DIC) analysis. In the case of FEA, the failure mode is visualised by the contour map of the crack strain perpendicular to the interface (Figure 6c, f). In the experimental testing program, the failure of the piers was confined to pier rocking and/or toe crushing, except for WS_0.5_2, which also displayed diagonal shear failure in the left pier. The FEA also showed the rocking failure of piers. In the case of spandrel failure, there was mixed shear and flexural failure in both the tested walls and FEA of the walls (despite this not showing clearly in Figure 6c due to the scale of the contour plot). With the increase of precompression level, the spandrel cracking was more prominent. The failure mode predicted by NZSEE (2006) was pier rocking (flexural failure) for all scenarios, while at higher precompression level NZSEE (2017) predicted that the failure mode transitioned to toe crushing. However, there was no distinction between the strengths associated with rocking and toe crushing in NZSEE (2006).

5.3 Maximum lateral load from test, FEA and NZSEE predictions

The maximum lateral load carrying capacity of the tested URM walls are compared to the predicted strengths from FEA and NZSEE equations (NZSEE, 2017; NZSEE, 2006) in Table 4. To determine the NZSEE predicted strengths, the effective pier height was taken by extending the straight portion of the pier up to the two-third height of the arch radius in the case of deep arches according to NZSEE (2017) such as the semi-circular arches used in this study. Also the pier was considered as fixed-fixed boundary conditions considering the spandrel with sufficient load and rotational resisting capacity. The

percentage difference of the maximum lateral load obtained from the FEA and NZSEE equation compared to the test results are presented in Table 4 in parentheses. The governing shear force (minimum value) equation numbers for NZSEE 2006 & 2017 are also presented in Table 4, which represent the predicted failure modes. The experimental maximum lateral load value for the walls presented in the Table 4 was obtained by averaging the maximum values in push and pull directions for both repeated walls.

By comparing the results, it was observed that the FEA results were in close agreement with the test data at both levels of precompression and the FEA more closely matched the experimentally measured strengths than the NZSEE predicted values. For the low precompression level the NZSEE equations provided a conservative strength prediction which was closer to the test result than for the high precompression level, the latter being non-conservative. The closer agreement at low precompression is believed to have resulted from the assumption of fixed-fixed boundary conditions for the piers. This boundary condition assumes that the spandrel remains relatively undamaged and is able to effectively couple the piers. As observed in the tested walls, this was true for the low precompression level. However, in the case of high precompression load, the spandrel damage was more evident. Hence for high precompression load, the tops of the piers may lose the fixity and resistance capacity provided by the spandrel, which can reduce the lateral load capacity of the wall as the boundary condition for the piers transitions towards cantilever (fixed-free) conditions.

6 Conclusions

This paper has focused on the seismic in-plane behaviour of unreinforced masonry walls with semi-circular arched openings representing heritage Australian masonry construction. To evaluate the seismic performance of the walls, pseudostatic cyclic in-plane tests of the specimens were performed with the combination of constant vertical and cyclic horizontal loading. The walls were analysed based on the load displacement behaviour and the failure modes. The same specimens were modelled using a micro-modelling approach in the commercially available finite element software package Diana 10.2. In addition, the shear capacity and the predicted failure modes of the walls were evaluated using the NZSEE predictions. The following conclusions can be summarised from the comparisons of the test, FEA and NZSEE.

- The vertical precompression level has significant influence on the seismic behaviour of URM walls. With the increase of the vertical stress on the wall, the lateral strength has increased but more damage was observed in the piers and spandrel.
- At low precompression level, cracking is more confined in the spandrel with pier rocking but for higher precompression level, the pier experienced both shear and flexural failure.
- The FEA model successfully captured the global in-plane behaviour of the walls and the maximum lateral strength is well matched with the experimental results. Although the crack patterns predicted by the model are not exactly in agreement with the test results, the FEA model successfully captured the expected failure

modes for three of the tested walls. The only exception was WD_0.5_2 which displayed shear failure in the left pier, this not being predicted by the FEA model.

- Also, good agreement was found for the lateral strength prediction according to the NZSEE with the test result for the low precompression level. But for higher precompression level, there is a marked difference between the NZSEE predicted strength and the test results. This is believed to relate to the greater degree of damage of the spandrel at higher precompression which was not captured in the way the NZSEE predictions were applied in this study.

References

- Allen, C., Masia, M. J., Page, A. W. (2014) Cyclic in-plane shear behaviour of unreinforced masonry walls with openings: Design of experimental testing programme. In *9th International Masonry Conference*, Guimarães, Portugal.
- Allen, C., Masia, M. J., Page, A. W., Griffith, M.C., Derakhshan, H. and Mojsilovic, N. (2016) Experimental testing of unreinforced masonry walls with openings subjected to cyclic in-plane shear. In *16th International Brick & Block Masonry Conference - IB²MAC*, Padova, Italy.
- Allen, C., Masia, M. J., Page, A. W., Griffith, M.C. and Ingham, J. (2017) Nonlinear finite element modelling of unreinforced masonry walls with openings subjected to in-plane shear. In *13th Canadian Masonry Symposium – CMS*, Halifax, Canada.
- AS2121 (1979) ‘The Design of Earthquake Resistant Buildings’, *Standards Australia Limited*, Homebush, Australia.
- AS/NZS 4456.4 (2003) ‘Masonry Units, Segmental Pavers and Flags-Methods of Test - Determining Compressive Strength of Masonry Units’, *Standards Australia Limited and Standards New Zealand*, Australia and New Zealand.
- AS/NZS 4456.15 (2003) ‘Masonry Units, Segmental Pavers and Flags-Methods of Test - Determining Lateral Modulus of Rupture’, *Standard Australia Limited and Standards New Zealand*, Australia and New Zealand.
- ASTM (2011) ‘Standard Test Method for Compressive Strength of Hydraulic Cement Mortars (using 2-in or 50-mm cube specimens)’, *ASTM C109/C 109M-11*, West Conshohocken, PA.
- AS 3700 (2018) ‘Masonry Structures’, *Standards Australia Limited*, Homebush, Australia.
- ASCE 41-13 (2014) ‘Seismic Evaluation of Existing Buildings’, *American Society of Civil Engineers and Structural Engineering Institute*, Virginia, USA.

Augenti, N., Parisi, F., Prota, A., and Manfredi, G. (2011) 'In-plane lateral response of a full-scale masonry subassemblage with and without an inorganic matrix-grid strengthening system', *Journal of Composites for Construction*, Vol. 15, No. 4, pp.578-590.

Beyer, K. (2012) 'Peak and residual strengths of brick masonry spandrels', *Engineering Structures*, Vol. 41, pp.533-547.

Beyer, K. and Dazio, A. (2012) 'Quasi-static cyclic tests on masonry spandrels', *Earthquake Spectra*, Vol. 28, No. 3, pp.907-929.

Betti, M., Galano, L., and Vignoli, A. (2014) 'Comparative analysis on the seismic behaviour of unreinforced masonry buildings with flexible diaphragms', *Engineering Structures*, Vol. 61, pp.195-208.

Bothara, J. K., Dhakal, R. P., and Mander, J. B. (2010) 'Seismic performance of an unreinforced masonry building: an experimental investigation', *Earthquake Engineering & Structural Dynamics*, Vol. 39, No. 1, pp.45-68.

Brencich, A., Gambarotta, L., and Lagomarsino, S. (1998) A macroelement approach to the three-dimensional seismic analysis of masonry buildings. In *11th European Conference on Earthquake Engineering*, Balkema, Rotterdam.

Calvi, G. M., Kingsley, G. R., and Magenes, G. (1996) 'Testing of masonry structures for seismic assessment' *Earthquake Spectra*, Vol. 12, No. 1, pp.145-162.

Diana FEA. (2017) 'DIANA Finite Element Analysis User's Manual Release 10.2', Delft, The Netherlands.

EN1052-3 (2002) 'Methods of Test for Masonry, Part 3: Determination of Initial Shear Strength', *European committee of Standardization*, Brussels.

Howlader, M. K., Masia, M. J., Griffith, M. C., Ingham, J. M. and Jordan, J. W. (2016) Characterisation of heritage masonry construction in NSW - State Heritage Register. In *Australian Earthquake Engineering Society conference*, Melbourne, Australia.

Howlader, M. K., Masia, M. J., Griffith, M. C. and Jordan, J. W. (2018) Design of in-plane unreinforced masonry wall testing program and preliminary finite element analysis (FEA). In *10th Australian Masonry Conference - AMC*, Sydney, Australia.

Knox, C. L. (2012) *Assessment of Perforated Unreinforced Masonry Walls Responding In-plane*, PhD Thesis, The University of Auckland, New Zealand.

Knox, C. L., Dizhur, D. and Ingham, J. M. (2017) 'Experimental cyclic testing of URM pier-spandrel substructures', *Journal of Structural Engineering*, Vol. 143, No. 2.

Lagomarsino, S., Penna, A., Galasco, A., and Cattari, S. (2013) 'TREMURI program: an equivalent frame model for the nonlinear seismic analysis of masonry buildings', *Engineering Structures*, Vol. 56, pp.1787-1799.

Lourenco, P. B. (1996a) *Computational Strategies for Masonry Structures*, PhD Thesis, Delft University of Technology (TU Delft), Netherlands.

Lourenco, P. B. (1996b) 'A user/programmer guide for the micromodeling of masonry structures TU-DELFT report no. 03.21.1.31.35: TNO Building and Construction Research, Computational Mechanics', Delft University of Technology & University of Minho.

Lourenco, P. B. (2008). Structural masonry analysis: Recent developments and prospects. In *14th international brick and block masonry conference - IB2MaC*, Sydney, Australia.

Magenes, G. and Calvi, G. M. (1997) 'In-plane seismic response of brick masonry walls', *Earthquake Engineering & Structural Dynamics*, Vol. 26, No. 11, pp.1091-1112.

Melchers, R., and Page, A. W. (1990) 'Preliminary report on Newcastle earthquake', *The University of Newcastle*, NSW 2308, Australia.

Moon, F. L., Yi, T., Leon, R. T. and Kahn, L. F. (2006) 'Recommendations for Seismic Evaluation and Retrofit of Low Rise URM Structures', *Journal of Structural Engineering*, Vol. 132, No. 5, pp.663-672.

Nateghi, F. A., and Alemi, F. (2008) Experimental study of seismic behaviour of typical Iranian URM brick walls. In *14th World Conference on Earthquake Engineering*. Beijing, China.

NZSEE (2006) 'Assessment and Improvement of the Structural Performance of Buildings in Earthquake -Prioritisation, Initial Evaluation, Detailed Assessment, Improvement Measures: Recommendations of a NZSEE Study Group on Earthquake Risk Buildings', *New Zealand Society for Earthquake Engineering*, New Zealand.

NZSEE (2017) 'The Seismic Assessment of Existing Buildings, Technical Guidelines for Engineering Assessments. Section C8- Seismic Assessment of Unreinforced Masonry Buildings', *New Zealand Society for Earthquake Engineering*, New Zealand.

Petersen, R. B. (2009) *In-plane Shear Behaviour of Unreinforced Masonry Panels Strengthened with Fibre Reinforced Polymer Strips*, PhD Thesis, School of Engineering, The University of Newcastle, Australia.

Russell, A. (2010) *Characterisation and Seismic Assessment of Unreinforced Masonry Buildings*, PhD Thesis, The University of Auckland, New Zealand.

Triller, P., Tomažević, M., and Gams, M. (2016) Seismic behaviour of multistorey plain masonry shear walls with openings: An experimental study. In *16th International Brick and Block Masonry Conference - IB²MAC*, Padova, Italy.

Vanin, A., and Foraboschi, P. (2012) 'In-plane behavior of perforated brick masonry walls', *Materials and Structures*, Vol. 45, No. 7, pp.1019-1034.

Yi, T., Moon, F. L., Leon, R. T., and Kahn, L. F. (2006) 'Lateral load tests on a two-story unreinforced masonry building' *Journal of Structural Engineering*, Vol. 132, No. 5, pp.643-652.

PERSONAL COPY

List of Figures

Figure 1 Geometry and layout of the tested walls (all dimensions are in mm)

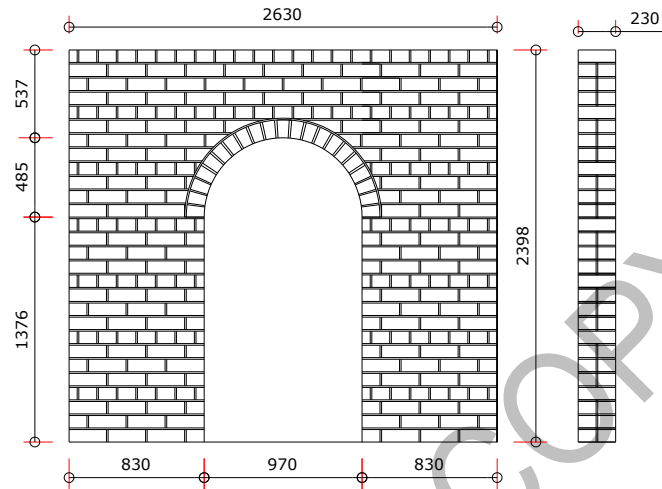


Figure 2 Test set-up and instrumentation (blue denotes absolute and black denotes relative displacement; H, V, X denotes horizontal, vertical and diagonal respectively)

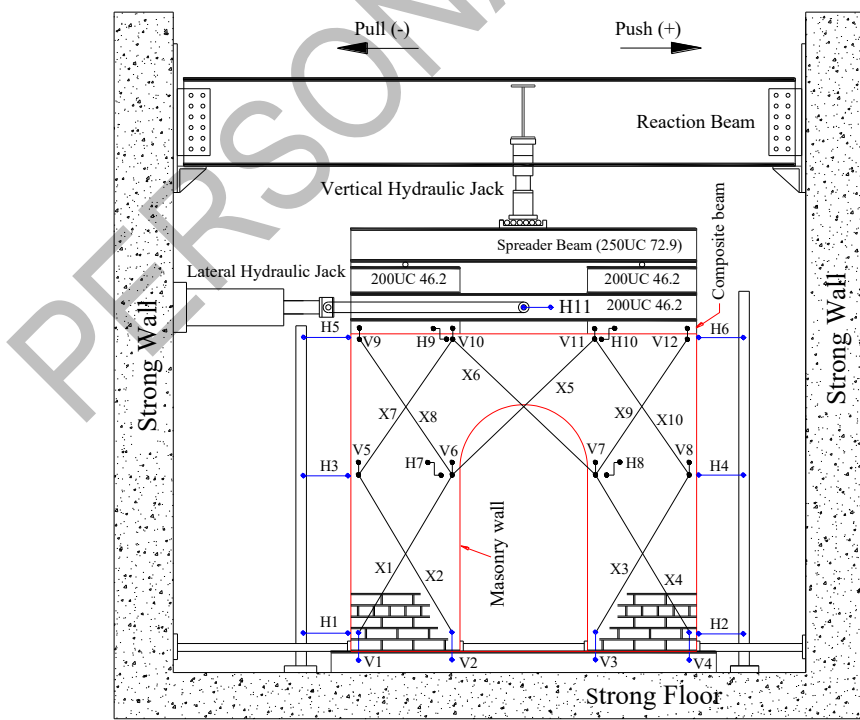


Figure 3 Imposed displacement (H11) time history for tests

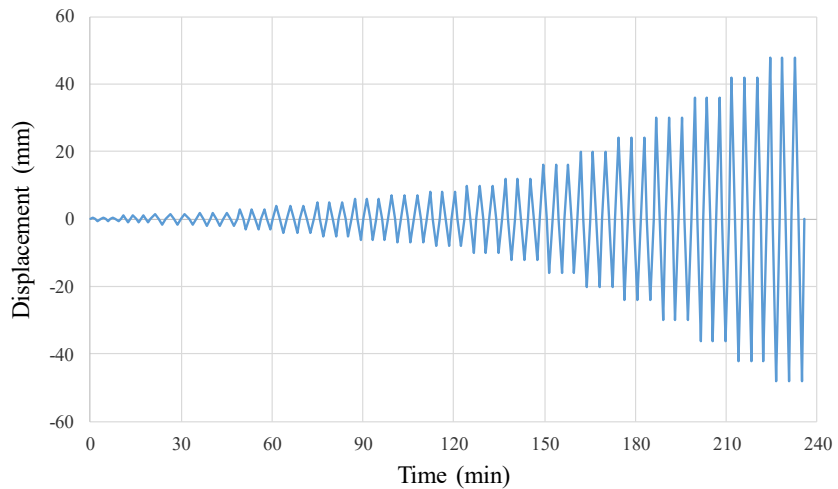


Figure 4 Force displacement hysteresis loops

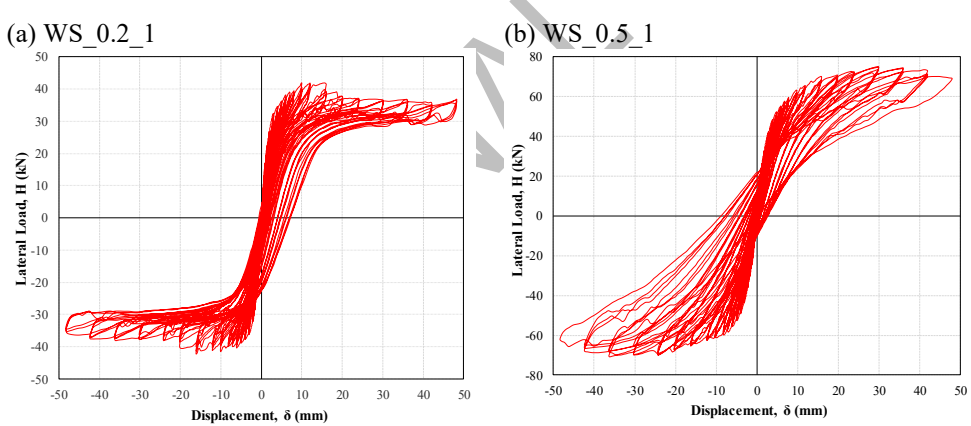


Figure 5 Force displacement plot for experimental and FEA results

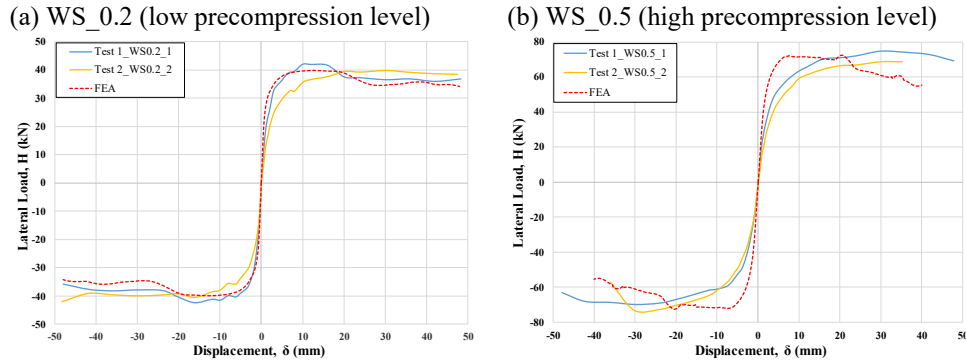
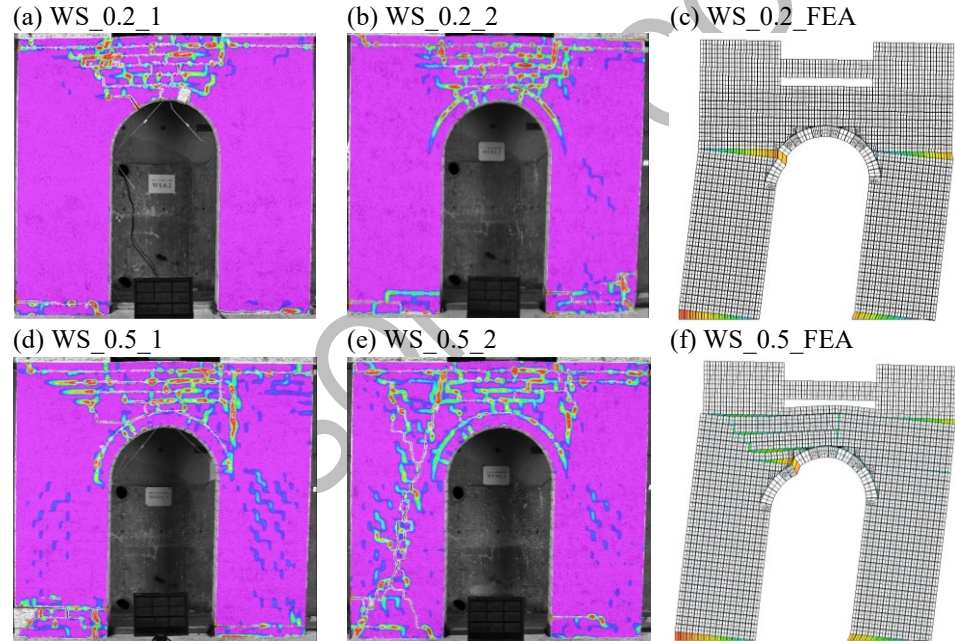


Figure 6 Crack patterns from tested walls and FEA results



List of Tables

Table 1 Material Properties

Parameters	Value	COV (%)	Unit	Test method
Brick compressive strength (f'_b)	13.6	6	MPa	AS/NZS4456.4 (2003)
Flexural tensile strength of brick (f'_{ut})	1.1	23	MPa	AS/NZS 4456.15 (2003)
Mortar compressive strength (f'_j)	1.7	2	MPa	ASTM C109/C109M-11 (2011)
Direct tensile strength of mortar joint (f_{jt})	See Table 2			AS3700 (2018)
Joint cohesion (c)	0.15	--	MPa	
Joint coefficient of friction ($\tan\varphi$)	0.74	--	--	EN 1052-3 (2002)
Masonry compressive strength (f'_m)	7.0	7	MPa	AS3700 (2018)

Table 2 Direct Tensile Strength of Mortar Joints

Wall Id	Batch No.	f'_{sp} (MPa)	COV (%)	f_{jt} (MPa)
WS_0.2_1	1	0.077	28	0.052
	2	0.146	22	0.073
WS_0.2_2	1	0.115	58	0.077
	2	0.094	29	0.063
WS_0.5_1	1	0.169	11	0.113
	2	0.201	17	0.134
WS_0.5_2	1	0.178	27	0.119
	2	0.179	18	0.119
Average of all wall		0.145	26	0.094

Table 3 Key material properties used in FE modelling

Material	Property	Value	Unit	Remarks
Brick	Young's modulus (E_b)	2502	MPa	Test
	Poisson's ratio (ν)	0.2	--	Assumed
	Tensile strength (f_{bt})	0.71	MPa	Test
	Tensile fracture energy (G_f^I)	0.021	N/mm	Lourenco (2008)
Steel	Young's modulus (E_{st})	200	GPa	Assumed
	Poisson's ratio (ν)	0.3	--	Assumed
Joint	Normal stiffness (k_n)	523	N/mm ³	Test
	Shear stiffness (k_s)	218	N/mm ³	Test
	Tensile strength (f_{jt})	0.097	MPa	Test
	Tensile fracture energy (G_f^I)	0.012	N/mm	Lourenco (1996 b)
	Cohesion (c_0)	0.15	--	Test
	Initial friction coefficient ($\tan\varphi_i$)	0.74	--	Test
	Initial dilatancy coefficient ($\tan\psi_0$)	0.50	--	Petersen (2009)
	Residual friction coefficient ($\tan\varphi_r$)	0.56	--	Petersen (2009)
	Confined normal stress (σ_u)	-0.75	MPa	Petersen (2009)
	Exponential degradation coefficient (δ)	1.8	--	Petersen (2009)
	Masonry compressive strength (f_c)	7.0	MPa	Test
	Compressive fracture energy (G_c)	11.2	N/mm	Test
	Shear traction control factor (C_s)	9.0	--	Lourenco (1996 b)
	Equivalent plastic relative displacement (κ_p)	0.0128	mm	Test
	Fracture energy factor (a) (G_f^{II})	-0.80	--	Petersen (2009)
	Fracture energy factor (b) (G_f^{II})	0.05	--	Petersen (2009)

Table 4 Summary of the maximum in-plane lateral loads of the walls

Wall ID	Experiment (kN)	FEA (kN)	NZSEE 2006		NZSEE 2017	
			(kN)	(kN)	(kN)	(kN)
WS_0.2	41.5	39.9 (-3.9%)	37.5 (-9.6%)	EQ 1	39.1 (-5.8%)	EQ 5
WS_0.5	71.6	72.4 (+1.1%)	86.7 (+21.1%)	EQ 1	88.1 (+23.0%)	EQ 6